Front. Mater. Sci. 2023, 17(4): 230660
https://doi.org/10.1007/s11706-023-0660-x

RESEARCH ARTICLE

A nonmulberry silk fibroin-based robust mandruka for rapid hemostasis treatment

Hao Zhang[1], Siyuan Luo[1], Weili Yang[1], Qisheng Luo[1], Perumal Ramesh Kannan[1], Yao Li (✉)[1,2], and Xiangdong Kong (✉)[1,2]

1 Institute of Smart Biomedical Materials, School of Materials Science and Engineering, Zhejiang Sci-Tech University, Hangzhou 310018, China
2 Zhejiang-Mauritius Joint Research Center for Biomaterials and Tissue Engineering, Zhejiang Sci-Tech University, Hangzhou 310018, China

ABSTRACT: Uncontrolled hemorrhage resulting from traumas causes severe health risks. There is an urgent need for expeditious hemostatic materials to treat bleeding incidents. Here, we developed a natural protein-based hemostatic sponge extracted from nonmulberry cocoons that exhibited rapid coagulation and effective absorption. We first built a degumming and dissolution system suitable for the *Dictyoploca japonica* cocoons to obtain regenerated silk fibroin (DSF). The DSF was then combined with carboxymethyl chitosan (CMCS) by glutaraldehyde (GA) crosslinking to ensure the structural stability of sponges. The resulting DSF–CMCS–GA exhibited remarkable hemostatic properties, displaying the highest absorption rate. It also demonstrated comparable efficacy to commercial hemostatic sponges. The blood-clotting index and hemolysis test showed that the prepared sponge possessed hemostatic activity and good hemocompatibility. Compared with mulberry silk fibroin hemostatic sponges (SF–CMCS–GA), DSF–CMCS–GA showed slightly better effects, making them a potential alternative to mulberry silk. In conclusion, our study introduces the use of *Dictyoploca japonica* silk fibroin for hemostasis, highlighting the exploitation of wild silkworm resources and providing an excellent silk fibroin-based hemostatic sealant for acute accident wounds and biomedical applications involving massive hemorrhage.

KEYWORDS: nonmulberry silk fibroin; *Dictyoploca japonica*; regenerated silk fibroin; hemostatic sponge

Contents

1 Introduction
2 Experimental
2.1 Materials
2.2 Degumming and dissolution system of *Dictyoploca japonica* silkworm cocoon
2.3 Degumming rate
2.4 Dissolving rate
2.5 Preparation of DSF–CMCS–GA
2.6 Characterization of sponges
2.7 Liquid absorption ratio of sponges
2.8 Hemostatic effect of DSF–CMCS–GA
2.9 Blood clotting indices
2.10 Hemolysis evaluation
2.11 Cytotoxicity test

Received June 6, 2023; accepted August 18, 2023

E-mails: kongxd@zstu.edu.cn (X.K.), liyao@zstu.edu.cn (Y.L.)

3 Results and discussion
3.1 Preparation of *Dictyoploca japonica* SF
3.2 Characterization of *Dictyoploca japonica* SF
3.3 Characterization of sponges
3.4 Hemostatic performance of sponges
3.5 Coagulation effect and hemocompatibility
4 Conclusions
Authors' contributions
Declaration of competing interests
Acknowledgements
Electronic supplementary information
References

1 Introduction

The amount of blood in the body is directly proportional to body weight and continuously flows and circulates within the cardiovascular system to provide an adequate supply of oxygen and nutrients [1]. It has been reported that blood loss reaches 20% of the total blood volume, blood circulation is impeded and this leads to a drop in blood pressure, resulting in symptoms like dizziness and reduced urine output. When the blood loss exceeds 40%, it can cause life-threatening conditions including cerebral hypoxia or shock if a timely blood transfusion is not administered [2–4]. Uncontrolled bleeding has become the second leading cause of trauma-related deaths in accidents, on the battlefield, and during surgical operations, accounting for 15% of trauma deaths [5–6]. Therefore, effective hemostasis plays a crucial role in controlling bleeding and significantly reducing mortality rates. Currently, the approaches of hemostasis involve vasoconstriction, platelet thrombosis, and blood clotting [7–8]. Many commercial hemostatic agents have been developed for rapid hemostasis, such as Curspon®, zeolite-based QuickClot®, Surgicel®, and fibrin-based bandages [9–10]. However, the existing hemostatic products have limitations, including poor hemostatic function, potential side effects, inadequate mechanical properties, and weak adhesion to tissue surfaces urge people to develop a safe, rapid, and effective hemostatic material to terminate bleeding problems.

Silk fibroin (SF), a natural protein material isolated from silkworm cocoons, has remarkable mechanical properties, biocompatibility, biodegradability, and easy availability, making it suitable for biomedical applications [11–13]. Over the past few decades, a wide range of SF-based biomaterials, including particles, films, nanofibrous mats, and three-dimensional (3D) scaffolds, have been extensively studied and developed [14–16]. In addition, SF has been used as a hemostatic agent in several studies. SF-based biomaterials have been extensively applied in various forms in different hemostatic applications [17–19]. The efficacy of degummed natural silk as a biomaterial for sutures and support structures led to its approval by the FDA for clinical use in 1993. Based on the source of silkworm species, SF can be divided into mulberry SF and nonmulberry SF. In recent years, there has been a growing interest among researchers in exploring nonmulberry SF. Nonmulberry silk has demonstrated comparable biocompatibility to mulberry silk in *in vivo* experiments [20–23]. Besides, nonmulberry SF contains unique peptide sequences, such as arginine-glycine-aspartic acid (RGD), which efficiently enhance cell adhesion and proliferation [24–26]. The β-sheet conformation in nonmulberry fibroin consists of abundant regular $(-\text{alanine}-)_n$ polypeptide sequence with higher binding energy, thereby imparting higher mechanical properties of nonmulberry fibroin-based biomaterials [27–28]. These inherent advantages have significantly promoted the development of excellent hemostatic agents based on nonmulberry fibroin.

Both mulberry silk and nonmulberry silk exhibit a distinct core–shell structure, comprising an inner core of SF and an outer sericin shell [29]. It has been reported that residual silk sericin can potentially induce immune rejection responses [30–31]. Therefore, the complete removal of silk sericin from silkworm cocoons is crucial to obtain immunogenic-free materials suitable for biomedical applications. The degumming and dissolution system for extracting SF from mulberry silkworms is well established [32]. However, the isolation procedure of nonmulberry SF remains unclear, posing a significant challenge in the development and utilization of nonmulberry SF in the field of biomedicine.

Herein, we present an effective strategy for achieving efficient hemostasis using a natural nonmulberry silk fibroin derived from a *Dictyoploca japonica* (DSF)-based sponge. The degumming and dissolution of the *Dictyoploca japonica* system suitable for SF isolation were optimized. Subsequently, the purified SF solution from *Dictyoploca japonica* was combined with carboxymethyl chitosan (CMCS) and formed a cross-linking network structure using glutaraldehyde (GA)

adhesive to fabricate a hemostatic sponge (DSF–CMCS–GA). The resulting sponge exhibited impressive liquid (phosphate buffered saline (PBS)) absorption capacity, rapid blood absorption rate, and effective blood coagulation performance. Interestingly, our prepared DSF–CMCS–GA showed comparable hemostatic effects on commercially available sponges. Moreover, it displayed reliable blood compatibility, offering a robust natural SF-based hemostatic sponge derived from nonmulberry sources, which provides a viable alternative for managing acute wounds or cases of severe hemorrhage.

2 Experimental

2.1 Materials

Sodium carbonate (Na_2CO_3), lithium hydroxide monohydrate ($LiOH·H_2O$), ammonium thiocyanate (NH_4SCN), calcium chloride ($CaCl_2$), CMCS, GA, and gelatin sponge were purchased from Aladdin Chemical Reagent Co., Ltd., Shanghai, China. Anticoagulated rabbit blood was procured from Beijing Bersee Science and Technology Co., Ltd. All the chemical reagents used in the studies were of analytical grade (AR), and the experimental water was ultrapure/deionized water.

2.2 Degumming and dissolution system of *Dictyoploca japonica* silkworm cocoon

The cocoons of *Dictyoploca japonica* were cut into small pieces and immersed in water for 1 h. Following this, the soaked cocoons were boiled in Na_2CO_3 solutions with various concentrations for 60 min. Subsequently, the silk fibers were subjected to washing with deionized water for three times and drying at a temperature of 60 °C to obtain the degummed *Dictyoploca japonica* silk fibers. The degummed silk fibers were treated with LiBr, $CaCl_2$, LiBr–urea, $ZnCl_2$, LiBr–$ZnCl_2$, $ZnCl_2$–ethanol–H_2O, and LiSCN solutions. These solutions were incubated at a temperature of 98 °C for a duration of 1 h to complete solubilization. Afterward, the SF solutions were dialyzed in dialysis bags (molecular weight (MW) cutoff 14 000) against deionized water for 3 d, with water changes every 8 h. The solutions were then centrifuged at 2500 $r·min^{-1}$ for 15 min, and the supernatant was collected and stored at 4 °C for further use. The concentration of the resulting solution was determined using the bicinchoninic acid (BCA) assay.

2.3 Degumming rate

To evaluate the removal of sericin from the cocoon of the *Dictyoploca japonica* silkworm, the degumming rate was calculated using Eq. (1):

$$\text{Degumming rate}/\% = \frac{M_b - M_a}{M_b} \times 100 \quad (1)$$

where M_b and M_a are weights of silk fibers before and after the degumming treatment, respectively. The experiments were conducted three times and the results were recorded.

2.4 Dissolving rate

The dissolving rate was used to evaluate the dissolution of silk fibers at various systems according to Eq. (2):

$$\text{Dissolving rate}/\% = \frac{M'_b - M'_a}{M'_b} \times 100 \quad (2)$$

where M'_b and M'_a are weights of silk fibers before and after the dissolution, respectively. The measurements were conducted three times and the results were recorded.

2.5 Preparation of DSF–CMCS–GA

The sponge was developed by combining the DSF solution with CMCS and crosslinking them using GA. In brief, 100 mL of the DSF solution (4% (w/v)) was mixed with 4 g CMCS and stirred at room temperature for 2 h. Subsequently, 0.2 mL GA was added to the solution and stirred for an additional 2 h at room temperature. The resulting mixture was then subjected to dialysis against deionized water for 3 d with regular changes of water. Finally, the pure mixture was pre-frozen at −80 °C for 4 h and then freeze-drying for 48 h.

2.6 Characterization of sponges

Morphological analysis was performed through scanning electron microscopy (SEM) by sputter-coating the sample with gold and capturing images using a Carl Zeiss Ultra 55 scanning electron microscope instrument, operated at an acceleration voltage of 3.00 kV. Fourier transform infrared spectroscopy (FTIR) was performed using the

Thermo Electron Scientific Nicolet 5700 instrument. X-ray diffraction (XRD) measurements were carried out in a scanning range from 5° to 45° at a scanning rate of 5(°)·min^{-1}.

2.7 Liquid absorption ratio of sponges

The liquid absorption capacity of sponges was assessed in both PBS and blood and quantified using the absorption rate. The liquid absorption rate of sponges in different liquid media was calculated using Eq. (3):

$$\text{Absorption rate}/\% = \frac{M_2 - M_1}{M_1} \times 100 \quad (3)$$

where M_1 was the weight of the sponges before absorbing liquid, and M_2 was the weight of the sponges after absorbing liquid. The experiments were conducted in triplicate.

2.8 Hemostatic effect of DSF–CMCS–GA

In the experiment, 50 mg of the sponge was placed in a 24-well plate. Subsequently, 1 mL of blood was added to each well. The absorption of blood in each group of sponges was photographed at different time intervals ranging from 1 to 4 min. For the hemostatic sponges, they were positioned at the center of a filter paper and then 500 μL of rabbit blood was added drop by drop onto the sponges. The area of each blood spot was measured when the blood no longer spread on the filter paper.

2.9 Blood clotting indices

The blood-clotting index (BCI) was evaluated following the previously reported method [33]. In brief, sponges weighing 40 mg were placed in 1.5 mL centrifuge tubes and maintained at a temperature of 37 °C for 10 min. Subsequently, 0.1 mL of blood and 0.02 mol·L^{-1} $CaCl_2$ solution were added to the tubes, and the mixture was incubated at 37 °C for 1, 2, 3, and 4 min, respectively. After the specified incubation time, the optical density (OD) of the sample was measured at 540 nm using a microplate reader. The blood with the $CaCl_2$ solution served as the blank control. The BCI value was calculated using the following equation:

$$\text{BCI}/\% = \frac{\text{OD}_{\text{sample}}}{\text{OD}_{\text{control}}} \times 100 \quad (4)$$

where $\text{OD}_{\text{sample}}$ represented the OD value of the sample, and $\text{OD}_{\text{control}}$ represented the OD value of the blank group. The experiments were conducted in triplicate.

2.10 Hemolysis evaluation

The hemolysis evaluation of DSF–CMCS–GA was performed according to the methodology described in the previous literature [34]. Briefly, 500 μL fresh blood was centrifuged at 1500 r·min^{-1} for 5 min. The resulting precipitate was washed and diluted 10 times with PBS. Subsequently, 10 mg DSF–CMCS–GA was incubated with 1 mL diluted blood at 37 °C for 1 h. Following the incubation period, the mixture was centrifuged at 1500 r·min^{-1} for 15 min. 100 μL supernatant was collected and the OD was measured at a wavelength of 545 nm using a microplate reader. PBS and deionized water were used as negative and positive controls, respectively. The hemolysis rate was then calculated using the following equation:

$$\text{Hemolysis rate}/\% = \frac{\text{OD}_{\text{experiment}} - \text{OD}_{\text{negative}}}{\text{OD}_{\text{positive}} - \text{OD}_{\text{negative}}} \times 100 \quad (5)$$

where $\text{OD}_{\text{experiment}}$ represented the OD value of the experimental group, $\text{OD}_{\text{positive}}$ represented the OD value of the positive control group, and $\text{OD}_{\text{negative}}$ represented the OD value of the negative control group. All the experiments were conducted in triplicate.

2.11 Cytotoxicity test

To evaluate the cytotoxicity of the samples, sponges were sterilized by ultraviolet disinfection for 4 h. Then, 20 mg of each group was soaked in 10 mL Dulbecco's modified Eagle medium (DMEM) with 10% fetal bovine serum (FBS) and 1% penicillin–streptomycin solution, followed by placement in an incubator for 12 h. Subsequently, the sponge supernatant was subjected to two rounds of filtration by a 0.5 μm strainer. The L929 planting density was 6000 cells per well in 96-well plants and then incubated for 24 h before replacing the original DMEM media with 200 μL sponge extracts of each group. The Cell Counting Kit-8 (CCK-8) solution was introduced into individual wells at 24 h time points. After incubation for 1 h, the wavelength of 490 nm was selected to test the absorbance.

3 Results and discussion

3.1 Preparation of *Dictyoploca japonica* SF

The extraction of natural regeneration silk fibroin (DSF) was carried out using nonmulberry silkworm cocoons of *Dictyoploca japonica* silkworm. Initially, a suitable degumming and dissolution system was developed for the *Dictyoploca japonica* silkworm cocoon. In this regard, a degumming method involving a Na_2CO_3 solution was chosen. To determine the optimal degumming parameters, different concentrations of Na_2CO_3 and various treatment durations were employed for treating the *Dictyoploca japonica* silkworm cocoon. In Fig. S1(A), we observed that the degumming rate of the cocoons gradually increased from (2.9±0.3)% to (26±1.4)% as the concentration of Na_2CO_3 increased from 0.5% to 3.5% (w/v). The degumming rate remained stable at approximately 27% and showed no significant change when the Na_2CO_3 concentration reached 2% (w/v), which was consistent with previous report [35]. As described in the literature, sericin constitutes 25%–30% of silk protein. Additionally, the optimal degumming time was determined. By using a Na_2CO_3 concentration of 2% (w/v), the degumming rate was monitored at different reaction durations. The degumming rate increased from (12.8±0.6)% to (27.4±0.4)% as the treatment time increased from 0.25 to 1.5 h. As shown in Fig. S1(B), the degumming rate reached a plateau period after 1 h incubation. We evaluated the morphological changes of cocoons under different Na_2CO_3 concentrations and various degumming durations using SEM. As depicted in Fig. 1(A), the fiber surface initially exhibited cracks and some attached granules, which could be attributed to the presence of residual silk sericin. However, as the Na_2CO_3 concentration or the incubation time increased, the fiber surface gradually became smooth and the fine lines appeared more uniform. Nevertheless, excessive degumming, resulting in broken and rough fibers, was observed at high concentrations of the degumming agent (> 3 wt.%) or longer treatment duration (> 1.25 h). Consequently, we established the optimal degumming conditions for *Dictyoploca japonica* silkworm cocoons as 2 wt.% Na_2CO_3 at 98 °C for 1 h, which were used for subsequent experiments.

To obtain the regenerated SF solution, we explored the dissolution system for the degummed *Dictyoploca japonica* silk fibers. We compared the dissolution rate and dissolution time (Fig. S2) and found that $ZnCl_2$–ethanol–H_2O in the molar ratio of 1:2:8, $ZnCl_2$–ethanol–H_2O (3:1:8) and LiSCN systems exhibited good dissolution profiles (Table S1). The dissolution rates achieved were 59%, 94%, and 95%, respectively, as shown in Fig. 1(B). Both the $ZnCl_2$–ethanol–H_2O (3:1:8) and the LiSCN systems dissolved silk fibers in less than 30 min. To purify the dissolved SF solution, we employed a dialysis purification process. The LiSCN system demonstrated effective purification capabilities. Therefore, we chose the LiSCN dissolution system for the preparation of regenerated SF from *Dictyoploca japonica* and used it for subsequent experiments. SEM images presented in Fig. 1(C) also confirmed the satisfactory performance of the LiSCN dissolution system to generate a SF solution.

3.2 Characterization of *Dictyoploca japonica* SF

Based on the favorable biocompatibility of SF, we utilized *Dictyoploca japonica*-derived regenerated SF to construct a hemostatic sponge in combination with CMCS and crosslinked using GA as shown in Fig. 2(A) (DSF–CMCS–GA). To investigate whether different dissolution systems would affect the intrinsic properties of SF, we compared the effects of LiSCN and $CaCl_2$ dissolution agents for the SF solution generation. As observed in SEM images presented in Fig. 2(B), both LiSCN and $CaCl_2$ showed the ability to dissolve silk fibers. However, the LiSCN agent displayed a more efficient dissolution capability, resulting in a lower distribution of fibers compared to $CaCl_2$ (Fig. 2(B)). Importantly, the different dissolution agents did not alter the structure of SF (Fig. 2(C)). XRD analyses revealed that all forms of SF exhibited broad peaks near 22°, indicating their amorphous structures. Furthermore, *Dictyoploca japonica* SF showed a distinctive diffraction peak near 11.8°, which can be attributed to its α-helix structure. The FTIR analysis confirmed that the chemical structure of SF remained unaffected by various dissolution agents (Fig. 2(D)). All the regenerated SF showed absorption peaks at 1650, 1540, and 1240 cm^{-1}, corresponding to amide I, amide II, and amide III, respectively.

3.3 Characterization of sponges

The hemostatic sponge was developed based on *Dictyoploca japonica* silk fibroin by combining with

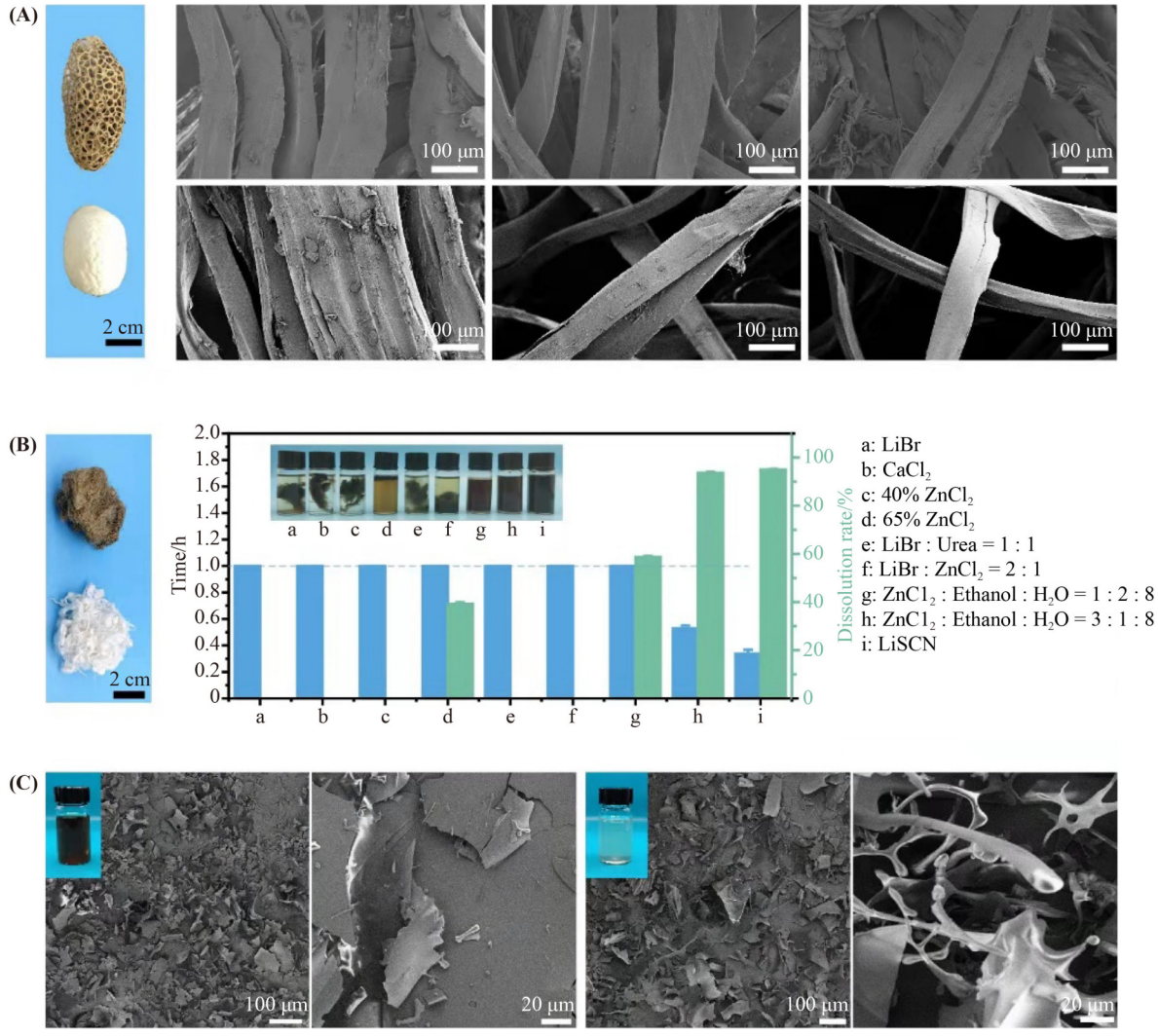

Fig. 1 The preparation of DSF. (**A**) The photograph of the silkworm cocoon, the *Dictyoploca japonica* (upper) and Mulberry (below), and SEM images of the cocoon with different degumming conditions. Different concentrations (upper) and different time (below). (**B**) The photograph of the silk after degumming, the *Dictyoploca japonica* (upper) and Mulberry (below), and the SF solution extraction procedure uses different solvent systems (n = 3). (**C**) SEM images of DSF and SF after dissolving in LiSCN. The inserted photograph shows the solubility of DSF (left) and SF (right).

CMCS and crosslinking using GA. The successful construction of the DSF–CMCS–GA sponge was confirmed by the FTIR spectrum, as shown in Fig. 2(E). CMCS exhibited four distinct absorption peaks at 1590, 1415, 1320, and 1060 cm^{-1}. When *Dictyoploca japonica* SF was mixed with CMCS, the absorption peaks at 1415 and 1320 cm^{-1} remained, while the absorption peaks at 1590 and 1060 cm^{-1} disappeared, indicating the influence of hydrogen bonding. Subsequently, the addition of the crosslinker GA caused the absorption peak at 1650 cm^{-1} to shift to 1620 cm^{-1}, indicating a transformation of the sponge structure from a random coil to a β-sheet conformation. It is widely recognized that the presence of β-sheet structure in proteins significantly enhances mechanical stability and silk hydration, making them favorable for liquid absorption, including blood.

SEM was conducted to evaluate different formulations of sponges, namely DSF–CMCS, DSF–CMCS–GA, SF–CMCS, SF–CMCS–GA, DSF–GA, and SF–GA. As seen in Fig. 3, both DSF–GA and SF–GA groups showed a lamellar structure. On the other hand, DSF–CMCS and SF–CMCS groups displayed a porous network distribution. Interestingly, DSF–CMCS–GA and SF–CMCS–GA groups showcased a staggered porous structure, characterized by regular shaped holes with uniform size that were distributed throughout the sponge.

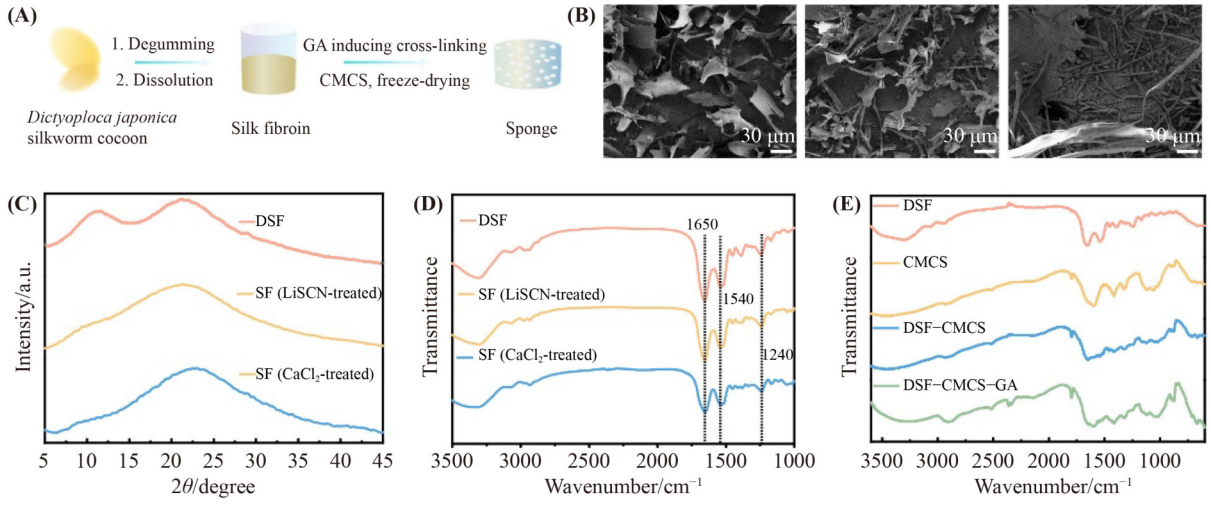

Fig. 2 (**A**) Schematic illustration for the preparation of SF-based sponge. (**B**) SEM images of LiSCN-treated DSF (left), LiSCN-treated SF (middle), and $CaCl_2$-treated SF (right). (**C**) XRD patterns of DSF and SF treated with LiSCN and $CaCl_2$ solvent systems. (**D**) FTIR spectra of DSF as well as SFs treated with LiSCN and $CaCl_2$ solvent systems, respectively. (**E**) Conformational analyses of sponges by FTIR spectroscopy.

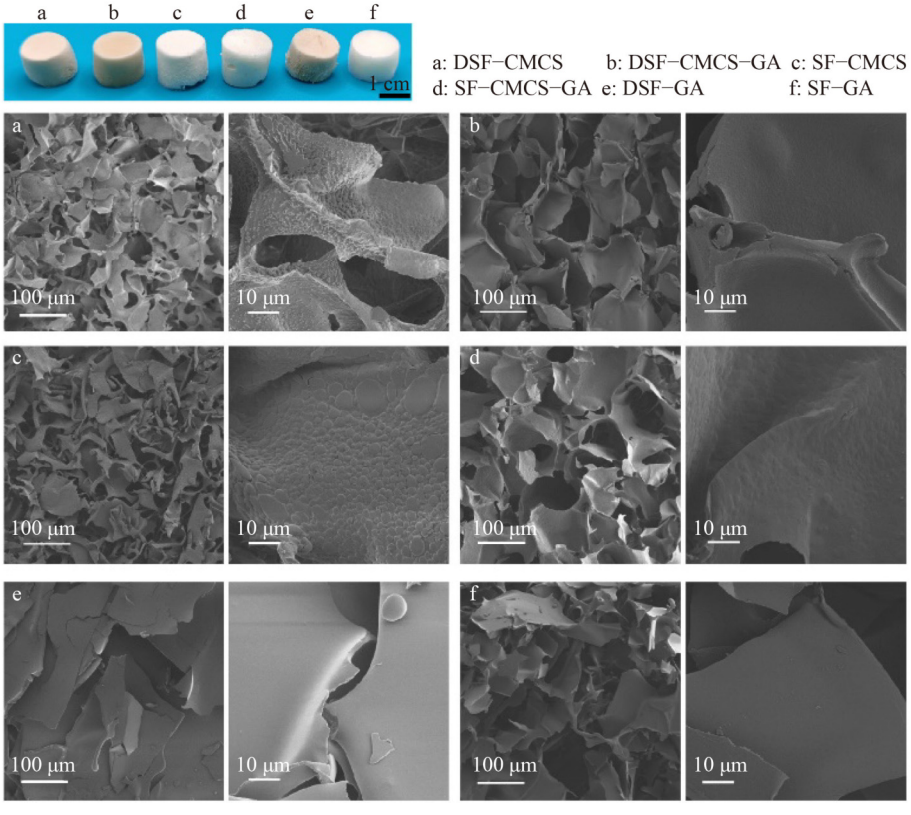

Fig. 3 Photographic images of DSF-based sponge. Representative SEM images show the microtopography of various formulations of SF-based sponge after lyophilization. The right side images show the magnified views.

3.4 Hemostatic performance of sponges

To assess potential biomedical applications of *Dictyoploca japonica* SF comparable to mulberry SF, the hemostatic effect of the DSF–CMCS–GA sponge was investigated. As a comparison group, sponges based on mulberry SF were also prepared. Considering the crucial role of liquid absorption in hemostasis, the solution

adsorption capability of the prepared sponges was evaluated using PBS and fresh rabbit blood. A commercially available gelatin sponge served as a positive control group. As the data shown in Figs. 4(A) and 4(B), the PBS absorption rates for each group were (164±35)%, (1885±269)%, (122±18)%, (1683±142)%, (210±42)%, (186±37)%, and (1553±447)%, respectively. Notably, the PBS absorption rate in DSF–CMCS–GA and SF–CMCS–GA groups was approximately 15 times higher than those of other groups and even exceeded that of the positive control group. Similarly, DSF–CMCS–GA and SF–CMCS–GA also exhibited superior blood absorption effect, with DSF–CMCS–GA achieving the highest blood absorption rate of (1293±108)% (Figs. 4(C) and 4(D)). Additionally, the blood absorption rate of the DSF–CMCS–GA or SF–CMCS–GA group is even higher than that of the gelatin sponge.

To directly visualize the hemostatic ability of the SF-based sponge, a blood absorption test was conducted using the filter method. As shown in Fig. 4(E), the DSF–CMCS–GA, SF–CMCS–GA, or Gel group absorbed rapidly and effectively prevented the spreading of blood. In addition, both DSF–CMCS–GA and SF–CMCS–GA hemostatic sponges showed sufficient mechanical properties to maintain their initial shape, which is advantageous for the removal of the sponge after hemostasis. The quantitative analysis of the diffusion areas further confirmed the superior hemostatic capacity of the DSF–CMCS–GA sponge (Fig. S3). Remarkably, DSF–CMCS–GA exhibited a slightly better blood absorption effect in preventing blood diffusion in a short time, when compared to mulberry SF-based (SF–CMCS–GA) or gelatin hemostatic sponge (positive control).

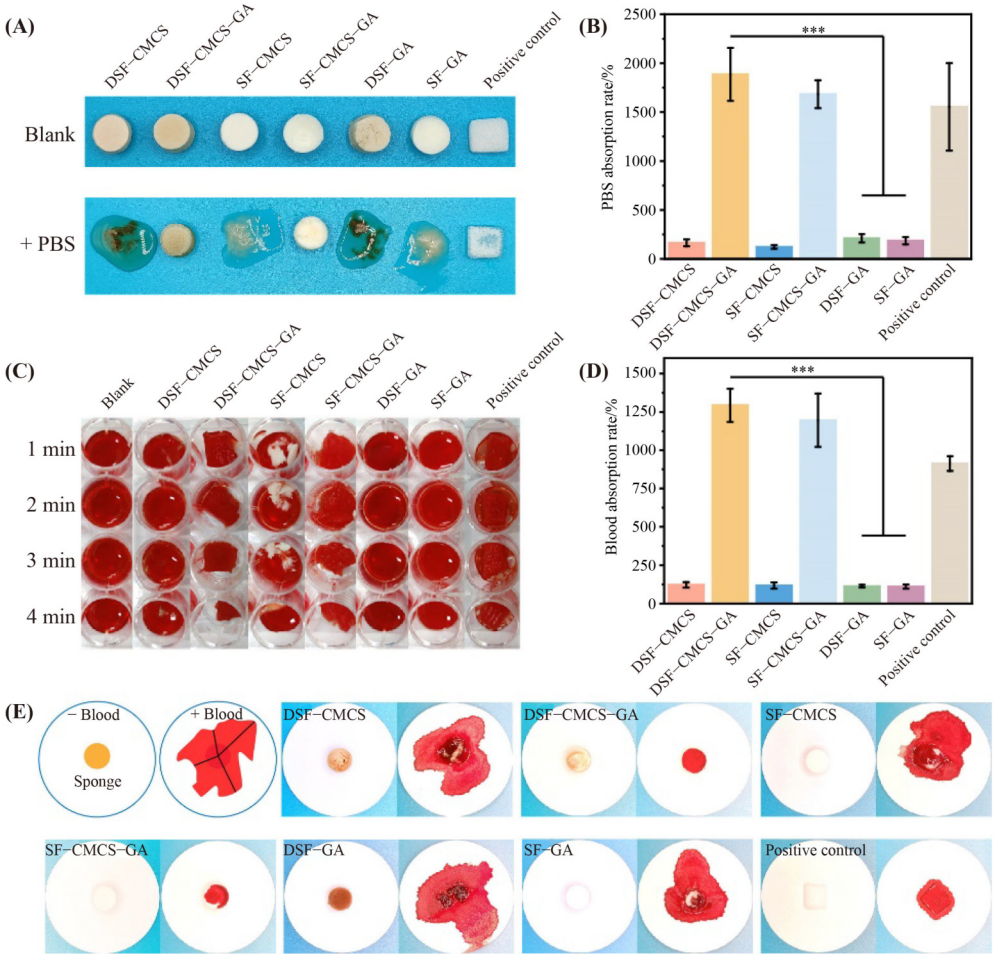

Fig. 4 DSF-based sponge for hemostasis. (**A**) Moisture absorption performance of SF-based hemostatic sponge and (**B**) the relative PBS absorption rate. (**C**) Clotting photographs of DSF–CMCS–GA after contact with blood for 1, 2, 3, and 4 min. (**D**) The quantitative blood absorption rate (n = 3). (**E**) Coagulation effect of DSF–CMCS–GA sponge after incubating with rabbit blood using filter-paper method.

3.5 Coagulation effect and hemocompatibility

The BCI is a vital indicator to evaluate the tightness of blood clot, formation, and directly reflects the hemostatic effect induced by a product [36]. A lower BCI value signifies an improved clotting effect and efficient hemostasis properties. Herein, the BCI of the *Dictyoploca japonica* SF-based sponge (DSF–CMCS–GA) was evaluated. As the data shown in Fig. 5(A), both DSF–CMCS–GA and SF–CMCS–GA groups showed lower indices than those of the groups without crosslinking agent (DSF–CMCS and SF–CMCS groups). Meanwhile, the BCI of DSF–CMCS–GA decreased significantly with the extended incubation time. Notably, the BCI values of both DSF–CMCS–GA and SF–CMCS–GA were even lower than that of the gelatin sponge (positive control), which is consistent with the results presented in Fig. 4.

The hemocompatibility of the prepared sponges was further assessed using a hemolysis assay. The results shown in Fig. 5(B) reveal that the hemolysis rates of all groups were below 5%, which demonstrate that the sponges meet the requirements of the hemolysis testing in clinical product applications. These data strongly indicate the successful construction of sponges based on a natural protein derived from silk cocoon, which exhibits superior hemostatic effects and good hemocompatibility.

The cytocompatibility of the hemostatic materials was further tested. Figure S4 shows that the cell viability of L929 cells incubated with various groups are more than 90%. These results revealed that the hemostatic sponges possess good cytocompatibility.

4 Conclusions

In summary, we have successfully developed a hemostatic biomedical application nonmulberry SF-based sponge with promising potential for hemostatic biomedical applications. We propose that SF derived from *Dictyoploca japonica* silkworm can serve as an important natural protein for manufacturing biomedical products. We extensively investigated the degumming and dissolution processes of the *Dictyoploca japonica* silkworm cocoon to extract a solution of regenerated SF. Through optimization, we established the optimal procedure involving the cocoon treatment with 2 wt.% Na_2CO_3 at 98 °C for 1 h and dissolution using LiSCN, which resulted in the preparation of pure regenerated SF. Characterizations of regenerated SF and the resulting hemostatic sponges derived from *Dictyoploca japonica* silkworm cocoon were carried out using techniques such as XRD, FTIR, SEM, and the blood absorption assay. The resulting hemostatic sponges exhibited satisfactory hemostatic effects even comparable to commercially available gelatin-based hemostatic sponges. Moreover, the hemostatic sponges showed well-defined hemocompatibility, and we presented an efficient hemostatic product based on a natural protein derived from the *Dictyoploca japonica* silkworm cocoon. This study expands biomedical applications of wild-type SF and provides a promising approach for the development of hemostatic agents.

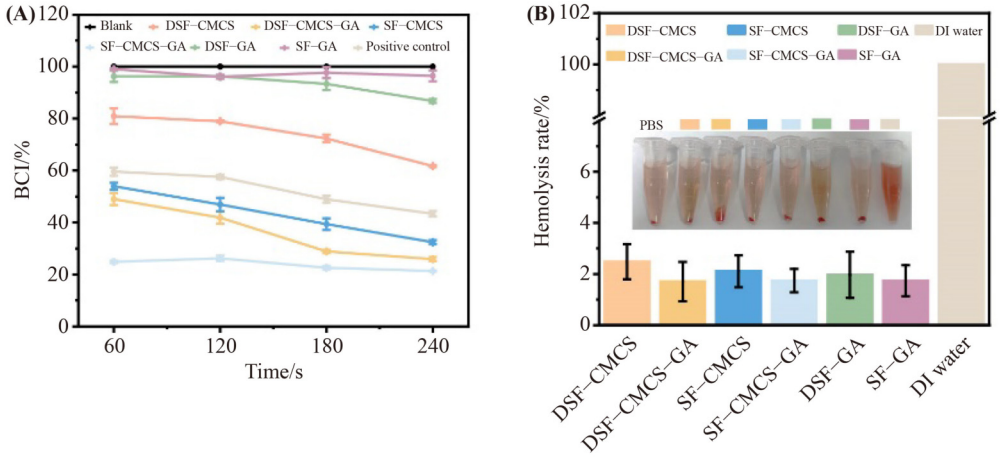

Fig. 5 Blood compatibility assay. (**A**) The BCI evaluation of DSF–CMCS–GA. (**B**) Hemolytic test of DSF–CMCS–GA. The inserted photograph shows the hemolysis performance. DI water was used as the positive control and PBS was the negative control ($n = 3$).

Authors' contributions H.Z., S.L., Y.L. and X.K. designed the research. H.Z., S.L., W.Y., Y.L. and X.K. performed the research. All authors analyzed and interpreted the data. Y.L., H.Z., P.R.K. and X.K. wrote and revised the paper.

Declaration of competing interests The authors declare that they have no competing interests.

Acknowledgements This research was financially supported by the National Natural Science Foundation of China (Grant Nos. 51672250, 32301177, and 51902289), the Key Research & Development Program of Zhejiang Province (Grant Nos. 2021C01180 and 2019C04020), and the Scientific Research Foundation of Zhejiang Sci-Tech University (Grant No. 22212238-Y).

Electronic supplementary information Supplementary materials can be found in the online version at https://doi.org/10.1007/s11706-023-0660-x and https://journal.hep.com.cn/foms/EN/10.1007/s11706-023-0660-x, which include Figs. S1–S4 and Table S1.

References

[1] Yu P Y, Zhong W. Hemostatic materials in wound care. Burns and Trauma, 2021, 9: tkab019

[2] Dries D J. The contemporary role of blood products and components used in trauma resuscitation. Scandinavian Journal of Trauma, Resuscitation and Emergency Medicine, 2010, 18(1): 63–80

[3] Khan M A, Mujahid M. A review on recent advances in chitosan based composite for hemostatic dressings. International Journal of Biological Macromolecules, 2019, 124: 138–147

[4] Hickman D A, Pawlowski C L, Sekhon U D S, et al. Biomaterials and advanced technologies for hemostatic management of bleeding. Advanced Materials, 2018, 30(4): 1700859

[5] Blackbourne L H, Baer D G, Eastridge B J, et al. Military medical revolution: prehospital combat casualty care. Journal of Trauma and Acute Care Surgery, 2012, 73(6): S372–S377

[6] Mabry R, Mcmanus J G. Prehospital advances in the management of severe penetrating trauma. Critical Care Medicine, 2008, 36(7 Suppl): S258–S266

[7] Zou C Y, Li Q J, Hu J J, et al. Design of biopolymer-based hemostatic material: starting from molecular structures and forms. Materials Today Bio, 2022, 17: 100468

[8] Malik A, Rehman F U, Shah K U, et al. Hemostatic strategies for uncontrolled bleeding: a comprehensive update. Journal of Biomedical Materials Research Part B: Applied Biomaterials, 2021, 109(10): 1465–1477

[9] Guo Y, Wang M, Liu Q, et al. Recent advances in the medical applications of hemostatic materials. Theranostics, 2023, 13(1): 161–196

[10] Wang L Y, You X R, Dai C L, et al. Hemostatic nanotechnologies for external and internal hemorrhage management. Biomaterials Science, 2020, 8(16): 4396–4412

[11] Rockwood D N, Preda R C, Yücel T, et al. Materials fabrication from *bombyx mori* silk fibroin. Nature Protocols, 2011, 6(10): 1612–1631

[12] Mushtaq A, Zhang H, Cui M Y, et al. ROS-responsive chlorin e6 and silk fibroin loaded ultrathin magnetic hydroxyapatite nanorods for T_1-magnetic resonance imaging guided photodynamic therapy *in vitro*. Colloids and Surfaces A: Physicochemical and Engineering Aspects, 2023, 656(Part B): 130513

[13] Cui T T, Yu J F, Li Q, et al. Large-scale fabrication of robust artificial skins from a biodegradable sealant-loaded nanofiber scaffold to skin tissue via microfluidic blow-spinning. Advanced Materials, 2020, 32(32): 2000982

[14] Yao X, Zou S Z, Fan S N, et al. Bioinspired silk fibroin materials: from silk building blocks extraction and reconstruction to advanced biomedical applications. Materials Today Bio, 2022, 16: 100381

[15] Qiao Z W, Lv X L, He S H, et al. A mussel-inspired supramolecular hydrogel with robust tissue anchor for rapid hemostasis of arterial and visceral bleedings. Bioactive Materials, 2021, 6(9): 2829–2840

[16] Luo D D, Yao C X, Zhang R, et al. Silk fibroin/collagen blended membrane fabricated via a green papermaking method for potential guided bone regeneration application: *in vitro* and *in vivo* evaluation. ACS Biomaterials Science & Engineering, 2021, 7(12): 5788–5797

[17] Dai M N, Li M, Gong J J, et al. Silk fibroin/gelatin/calcium alginate composite materials: preparation, pore characteristics, comprehensive hemostasis *in vitro*. Materials & Design, 2022, 216: 110577

[18] Lee J, Choi H N, Cha H J, et al. Microporous hemostatic sponge based on silk fibroin and starch with increased structural retentivity for contact activation of the coagulation cascade. Biomacromolecules, 2023, 24(4): 1763–1773

[19] Biswas S, Bhunia B K, Janani G, et al. Silk fibroin based formulations as potential hemostatic agents. ACS Biomaterials Science & Engineering, 2022, 8(6): 2654–2663

[20] Mehrotra S, de Melo B A G, Hirano M, et al. Nonmulberry silk based ink for fabricating mechanically robust cardiac patches and endothelialized myocardium-on-a-chip application. Advanced Functional Materials, 2020, 30(12): 1907436

[21] Sapru S, Das S, Mandal M, et al. Prospects of nonmulberry silk protein sericin-based nanofibrous matrices for wound healing — *in vitro* and *in vivo* investigations. Acta Biomaterialia, 2018, 78: 137–150

[22] Naskar D, Ghosh A K, Mandal M, et al. Dual growth factor loaded nonmulberry silk fibroin/carbon nanofiber composite 3D

scaffolds for *in vitro* and *in vivo* bone regeneration. Biomaterials, 2017, 136: 67–85

[23] Sahu N, Baligar P, Midha S, et al. Nonmulberry silk fibroin scaffold shows superior osteoconductivity than mulberry silk fibroin in calvarial bone regeneration. Advanced Healthcare Materials, 2015, 4(11): 1709–1721

[24] Zou S Z, Yao X, Shao H L, et al. Nonmulberry silk fibroin-based biomaterials: impact on cell behavior regulation and tissue regeneration. Acta Biomaterialia, 2022, 153: 68–84

[25] Mehrotra S, Nandi S K, Mandal B B. Stacked silk–cell monolayers as a biomimetic three dimensional construct for cardiac tissue reconstruction. Journal of Materials Chemistry B: Materials for Biology and Medicine, 2017, 5(31): 6325–6338

[26] Zou S Z, Wang X R, Fan S N, et al. Fabrication and characterization of regenerated *antheraea pernyi* silk fibroin scaffolds for schwann cell culturing. European Polymer Journal, 2019, 117: 123–133

[27] Fang G Q, Sapru S, Behera S, et al. Exploration of the tight structural–mechanical relationship in mulberry and non-mulberry silkworm silks. Journal of Materials Chemistry B: Materials for Biology and Medicine, 2016, 4(24): 4337–4347

[28] Zhou C Z, Confalonieri F, Medina N, et al. Fine organization of *bombyx mori* fibroin heavy chain gene. Nucleic Acids Research, 2000, 28(12): 2413–2419

[29] Holland C, Numata K, Rnjak-Kovacina J, et al. The biomedical use of silk: past, present, future. Advanced Healthcare Materials, 2019, 8(1): 1800465

[30] Vepari C, Kaplan D L. Silk as a biomaterial. Progress in Polymer Science, 2007, 32(8–9): 991–1007

[31] Ode Boni B O, Bakadia B M, Osi A R, et al. Immune response to silk sericin–fibroin composites: potential immunogenic elements and alternatives for immunomodulation. Macromolecular Bioscience, 2022, 22(1): 2100292

[32] Wang H Y, Wei Z G, Zhang Y Q. Dissolution and regeneration of silk from silkworm *bombyx mori* in ionic liquids and its application to medical biomaterials. International Journal of Biological Macromolecules, 2020, 143: 594–601

[33] Bian X Y, Cui C Y, Qi Y, et al. Amino acid surfactant-induced superfast gelation of silk fibroin for treating noncompressible hemorrhage. Advanced Functional Materials, 2022, 32(44): 2207349

[34] Zhang Y B, Wang H J, Raza A, et al. Preparation and evaluation of chitosan/polyvinylpyrrolidone/zein composite hemostatic sponges. International Journal of Biological Macromolecules, 2022, 205: 110–117

[35] Zhang Y Q. Applications of natural silk protein sericin in biomaterials. Biotechnology Advances, 2002, 20(2): 91–100

[36] Fan L H, Yang H, Yang J, et al. Preparation and characterization of chitosan/gelatin/PVA hydrogel for wound dressings. Carbohydrate Polymers, 2016, 146: 427–434